ACS Medicinal Chemistry Letters

pubs.acs.org/acsmedchemlett Letter

Identification of BRaf-Sparing Amino-Thienopyrimidines with Potent IRE1α Inhibitory Activity

Ramsay E. Beveridge,* Heidi Ackerly Wallweber, Avi Ashkenazi, Maureen Beresini, Kevin R. Clark, Paul Gibbons, Elise Ghiro, Susan Kaufman, Alexandre Larivée, Melissa Leblanc, Jean-Philippe Leclerc, Alexandre Lemire, Cuong Ly, Joachim Rudolph, Jacob B. Schwarz, Sanjay Srivastava, Weiru Wang, Liang Zhao, and Marie-Gabrielle Braun*

Cite This: https://dx.doi.org/10.1021/acsmedchemlett.0c00344 Read Online

ACCESS | Metrics & More | Article Recommendations | Supporting Information

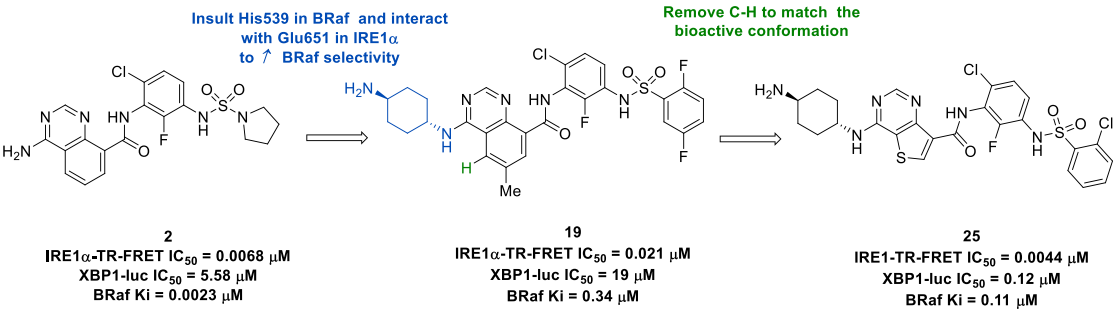

ABSTRACT: Amino-quinazoline BRaf kinase inhibitor **2** was identified from a library screen as a modest inhibitor of the unfolded protein response (UPR) regulating potential anticancer target IRE1α. A combination of crystallographic and conformational considerations were used to guide structure-based attenuation of BRaf activity and optimization of IRE1α potency. Quinazoline 6-position modifications were found to provide up to 100-fold improvement in IRE1α cellular potency but were ineffective at reducing BRaf activity. A salt bridge contact with Glu651 in IRE1α was then targeted to build in selectivity over BRaf which instead possesses a histidine in this position (His539). Torsional angle analysis revealed that the quinazoline hinge binder core was ill-suited to accommodate the required conformation to effectively reach Glu651, prompting a change to the thienopyrimidine hinge binder. Resulting analogues such as **25** demonstrated good IRE1α cellular potency and imparted more than 1000-fold decrease in BRaf activity.

KEYWORDS: *IRE1α, BRaf, kinase, unfolded protein response*

The unfolded protein response (UPR) is a cytoprotective protein synthesis homeostasis mechanism that is triggered by the accumulation of unfolded proteins in the endoplasmic reticulum (ER).[1] In the event of UPR signaling disruption, or extreme ER unfolded protein stress, the cellular apoptosis mechanism is activated, leading to cell death.[2−4] Many neoplastic disorders (e.g., multiple myeloma) have a high protein synthesis burden and rely heavily on specific branches of the UPR, particularly inositol requiring enzyme 1-alpha (IRE1α), to avoid the apoptosis cascade and survive.[5−7] As a result, selective interference with the UPR machinery is a potentially attractive approach to initiate caspase-mediated death of cancer cells and thus constitutes a promising strategy toward the discovery of novel cancer therapeutics.[8]

Management of the UPR is governed by three main branches which control transcriptional response mechanisms.[1] Among these, IRE1α is a bifunctional ER transmembrane sensor protein with kinase and RNase activity which regulates the most highly conserved branch of the UPR. In the event of unfolded protein stress in the ER, IRE1α undergoes dimerization/oligomerization and autophosphorylation which activates the transcription factor X-box binding protein 1 (XBP1). The ensuing splicing of XBP1 results in transcription of UPR genes and expression of ER chaperone proteins which restore normal cellular protein synthesis and trigger degradation of excessive unfolded protein.[9] For these reasons, it has been proposed that inhibition of IRE1α dimerization/oligomerization and endonuclease activity could be an attractive strategy to selectively disrupt the UPR in cancer cells and trigger the apoptosis cascade.[10−12] In particular, IRE1α

Received: June 23, 2020
Accepted: October 2, 2020

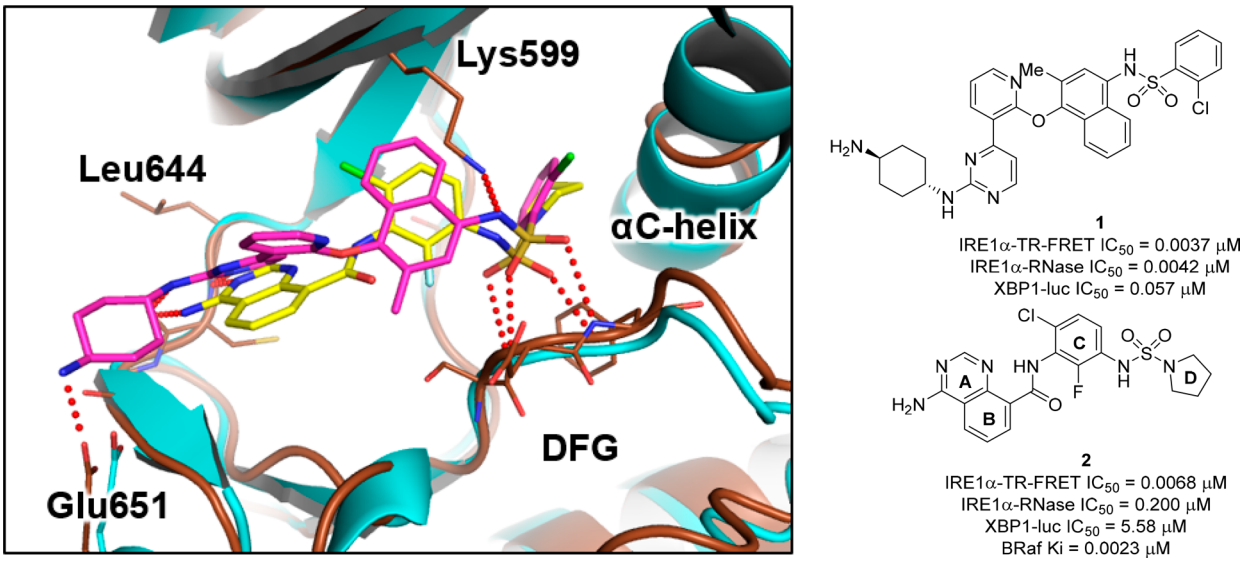

Figure 1. X-ray cocrystal structure of ligand **2** (yellow) identified from a Genentech internal kinase library screen (cyan = receptor of **2**, PBD code 6XDF, 2.54 Å) overlaid with compound (**1**) (pink) in hIRE1 (brown = receptor of **1**, PDB code 4U6R, 1.90 Å).

represents a rational target for multiple myeloma, because it regulates ER-associated degradation of misfolded proteins as well as secretion of several cytokines and chemokines known to be important for survival of malignant plasma cells in the bone marrow microenvironment.[13−15] As a consequence, there has been considerable interest toward discovery of small molecule inhibitors of IRE1α endonuclease activity.[16−20]

Table 1. 6-Me-Quinazoline Improves XBP1 Potency[a]

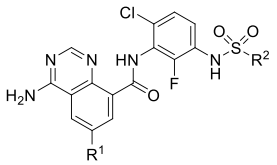

compd	R^1	IRE1α-TR-FRET IC_{50} (μM)	IRE1α-RNase IC_{50} (μM)	XBP1-luc IC_{50} (μM)	BRaf K_i (μM)
3	H	0.0089	0.056	12.7	-
4	Me	0.005	0.031	1.1	≤0.00008

[a]Data represent an average of ≥2 separate determinations. See the Supporting Information for standard deviations.

Interestingly, it has been shown that interference of IRE1α RNase activity can be allosterically controlled through targeting of the enzyme's C-terminal kinase domain.[21−24] For example, Harrington and co-workers at Amgen recently disclosed a potent and selective inhibitor of IRE1α RNase activity which binds to the IRE1α kinase domain (**1**, Figure 1).[24] Notably, the crystal structure of (**1**) in hIRE1α suggests that kinase domain binding with this ligand results in a conformational shift of the αC-helix resulting in reduced capacity of the enzyme to undergo crucial RNase active dimerization and oligomerization.

Our interest in exploring IRE1α as an anticancer target prompted an internal kinase focused screen toward identifying IRE1α RNase inhibitors. A total of 92K compounds were screened and these efforts initially identified compound **2** (Figure 1) as a promising hit from a prior amino-quinazoline BRaf kinase inhibitor program[25] with potent ATP-competitive IRE1α binding affinity (IRE1α-TR-FRET IC_{50} = 0.0068 μM). Compound **2** also demonstrated a modest inhibitory effect on IRE1α endonuclease activity as measured in both an enzymatic RNase inhibition assay (IRE1α-RNase IC_{50} = 0.200 μM) and a cellular X-box binding protein-1 splicing luciferase reporter assay (XBP1-luc IC_{50} = 5.58 μM). A crystal structure of **2** bound to IRE1 was obtained which showed that this ligand binds to the kinase domain ATP pocket in a similar fashion as ligand **1** with amino-quinazoline A-ring hinge contacts, sulfonyl urea DFG-motif binding, and pyrrolidine D-ring occupation of the αC-helix pocket (Figure 1). Some unique features of **2** include the absence of a polar headgroup salt bridge contact with Glu651, the existence of a pseudoring by intramolecular H-bonding between the N−H proton of the amide group and the one of nitrogen atoms on the quinazoline, and the presence of a new pocket close to the P-loop region of the quinazoline B-ring.

Based on compound **2**, a program was initiated to improve cellular potency of this starting point. Our primary goals for this series were to improve potency for IRE1α and reduce BRaf kinase binding affinity (BRaf K_i = 0.0023 μM). Using structure guided variation of core substituents and core replacement strategies; we were ultimately able to achieve both objectives as elaborated in the following part.

To drive our efforts, four assays were routinely used to evaluate compounds for their IRE1α and BRaf activities: IRE1α-TR-FRET was used to measure ATP-competitive IRE1α kinase binding potency; IRE1α -RNase was used to measure enzymatic endonuclease inhibition via cleavage of the XBP1 stem loop; XBP1 provided a cellular luciferase read-out of functional IRE1α-RNase inhibitory activity; and BRaf K_i values were determined in a kinase activity assay to evaluate potency against the key BRaf kinase antitarget. While the IRE1α-TR-FRET binding assay was routinely run to ensure ATP-competitive binding of new ligands to this kinase, the relatively high enzyme concentration required in this assay unfortunately resulted in an inability to discriminate between compound potencies below the enzyme concentration (less than ~10 nM). One consequence of this limitation was that a direct comparison of BRaf and IRE1α binding potencies could not be used as a

https://dx.doi.org/10.1021/acsmedchemlett.0c00344
ACS Med. Chem. Lett. XXXX, XXX, XXX−XXX

Table 2. Representative Amino-Quinazoline B-Ring and D-Ring SAR[a]

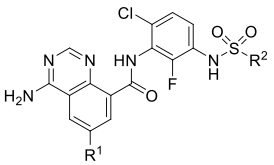

Compound	R^1	R^2	IRE1α-TR-FRET IC_{50} (μM)	IRE1α - RNase IC_{50} (μM)	XBP1-luc IC_{50} (μM)	BRaf Ki (μM)
(5)		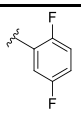	0.0033	0.033	1.6	-
(6)		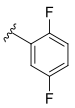	0.0037	0.047	4.9	≤ 0.00008
(7)		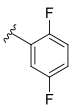	0.0055	0.076	3.2	-
(8)		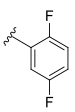	0.0053	0.050	0.28	-
(9)		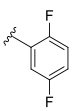	0.0051	0.053	2.0	-
(10)	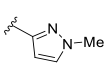	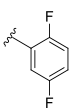	0.0078	0.089	1.7	-
(11)	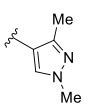	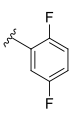	0.0049	0.082	0.15	-
(12)	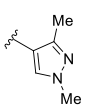		0.0071	0.064	0.048	0.00025[b]
(13)	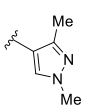		0.0053	0.040	0.044	≤ 0.00008[b]

[a]Data represent an average of ≥2 separate determinations. See the Supporting Information for standard deviations. [b]The potency was determined once.

rigorous selectivity metric. Nevertheless, the relative magnitudes of the BRaf K_i values among compounds still served as a useful metric to identify features which display BRaf sparing character toward our goal of identifying an IRE1α-selective ligand. In addition, IRE1α RNase assay data presents similar limitations in its ability to discriminate compounds with potencies better than 10 nM. Ultimately, the cellular XBP1 luciferase assay was deemed the most sensitive discriminator of functional RNase ligand potency, and as a result, our design efforts toward improving IRE1α inhibitory activity were guided primarily by activity in the XBP1 assay.

To further explore the potential impact of αC-helix shift on IRE1α potency, our attention first turned to examining additional amino-quinazoline BRaf ligands from our database with D-ring modifications that could push the αC-helix. Interestingly, this effort instead revealed a 6-Me-quinazoline B-ring substituent as a promising lead toward improved cellular XBP1 potency (Table 1). Structurally, this methyl group appeared to occupy a previously unexplored pocket close to

https://dx.doi.org/10.1021/acsmedchemlett.0c00344
ACS Med. Chem. Lett. XXXX, XXX, XXX−XXX

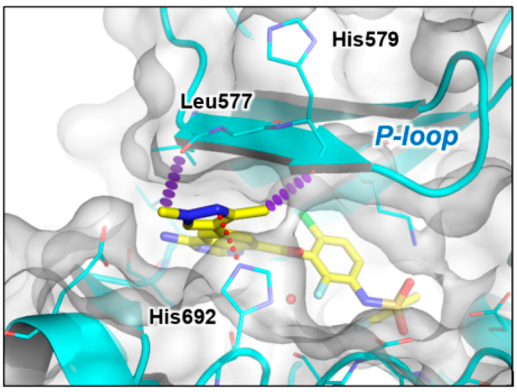

Figure 2. X-ray cocrystal structure of ligand **13** (yellow) in hIRE1α showing dimethyl-pyrazole quinazoline substituent interacting with P-loop residue Leu577 and His579 (PBD = 6XDB, 2.45 Å).

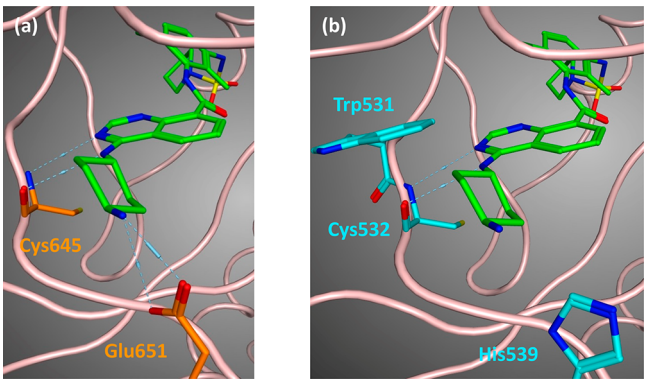

Figure 3. (a) Model of compound **2** with a *trans*-diaminocyclohexyl group attached to the quinazoline A-ring amine in IRE1α (orange) showing predicted salt bridge formation with Glu651. (b) Model of **2** with a *trans*-diaminocyclohexyl group attached to the quinazoline A-ring amine in BRaf (cyan). Green structure = compound **2**.

Table 3. Quinazoline A-Ring Polar Head Group SAR[a]

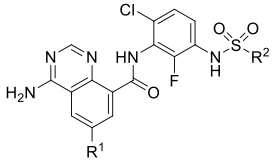

Compound	R^1	IRE1α-TR-FRET IC_{50} (μM)	IRE1α-RNase IC_{50} (μM)	XBP1-luc IC_{50} (μM)	BRaf Ki (μM)
15		0.40	5.5	29	-
16		0.058	0.92	31	0.0052[b]
17		0.21	3.5	19	0.070[b]
18		0.14	0.67	9.9	-
19		0.021	0.70	19	0.34[b]

[a]Data represent an average of ≥2 separate determinations. See the Supporting Information for standard deviations. [b]The potency was determined once.

the P-loop which we then sought to exploit toward further gains in IRE1α potency.

To guide our design efforts, analysis of the crystal structure of **2** indicated that this quinazoline B-ring is surrounded by polar residues and provides sufficient space to accommodate larger alkyl groups including 5- or 6-membered ring systems. Moreover, the imidazole ring of the His692 residue on the P-loop appeared to be ∼4−5 Å away from the quinazoline 6-position, suggesting incorporation of quinazoline substituents that could π-stack or hydrogen bond with this imidazole side chain could improve affinity. Altogether, these observations prompted an initial design strategy that focused on deploying heterocycles in this region to match the polar nature of this pocket while also targeting placement of aryl π-systems and heteroatoms in close proximity to the His692 imidazole ring. Specifically, combination of the quinazoline substituted with heterocycles at the 6-position and containing aryl sulfonamide D-rings was deemed an attractive strategy toward improving cellular XBP1 potency since such analogues appeared enabled for rapid structure−activity relationship (SAR) evaluation and were not predicted to interfere with the key kinase domain polar binding contacts.

We first explored incorporation of pyridines in this quinazoline pocket, which did not lead to improved XBP1 activity but appeared tolerated, providing an initial validation that aromatic heterocycles could be accommodated in this space (Table 2, compounds **5** and **6**). As a next step, 5-membered aromatic heterocycles were investigated leading to the identification of *N*-Me pyrazole **8** as a promising hit toward improved cellular potency and a potential proof-of-concept for interacting specifically with the His692 imidazole. Other *N*-Me pyrazole regioisomers **9** and **10** and desmethyl pyrazole **7** showed poor XBP1-luc potency which supported the possible existence of a directionally important hydrogen bond accepting interaction from His692. Next, further tuning of this 3-methyl pyrazole group with additional methyl substitutions distinguished the 4-quinazoline-1,3-dimethyl-pyrazole **11** as optimal for potency gains. In the end, exploration of the 1,3-dimethyl-pyrazole quinazoline feature in combination with other D-ring aryl sulfonamide groups resulted in the identification of compounds with up to 500-fold improvement in XBP1-luc cellular potency relative to the initial library hit **2** (Table 2, compounds **12**−**14**). To rationalize these potency gains, a crystal structure of 4-quinazoline-1,3-dimethyl-pyrazole ligand **13** in hIRE1α was obtained, which shows the pyrazole group engaging in a hydrogen bonding interaction with the imidazole of His692 (Figure 2). In addition, the two methyl groups engage in weak C−H hydrogen bonding interactions with the backbone carbonyl oxygen of Leu577 and His579.

While the results in Table 2 illustrate significant IRE1α cellular potency gains, it was disappointing to observe that these quinazoline B-ring modifications failed to show any meaningful decrease in BRaf kinase activity. To address this, we next considered the potential of targeting a salt bridge contact with a nonconserved residue Glu651 in IRE1α as a strategy to build in selectivity over BRaf kinase as this residue is a histidine (His539) in BRaf. A basic amine, while forming a salt bridge with Glu651, was expected to be repulsed by His539 in BRaf, or at least not engage in an attractive interaction. Encouragingly, structural models which transposed the *trans*-diaminocyclohexane group from **1**, a compound exhibiting minimal BRaf inhibition, onto quinazoline **2** in both IRE1α and BRaf appeared to support this selectivity approach (Figure 3). In IRE1α, we were pleased to

https://dx.doi.org/10.1021/acsmedchemlett.0c00344
ACS Med. Chem. Lett. XXXX, XXX, XXX−XXX

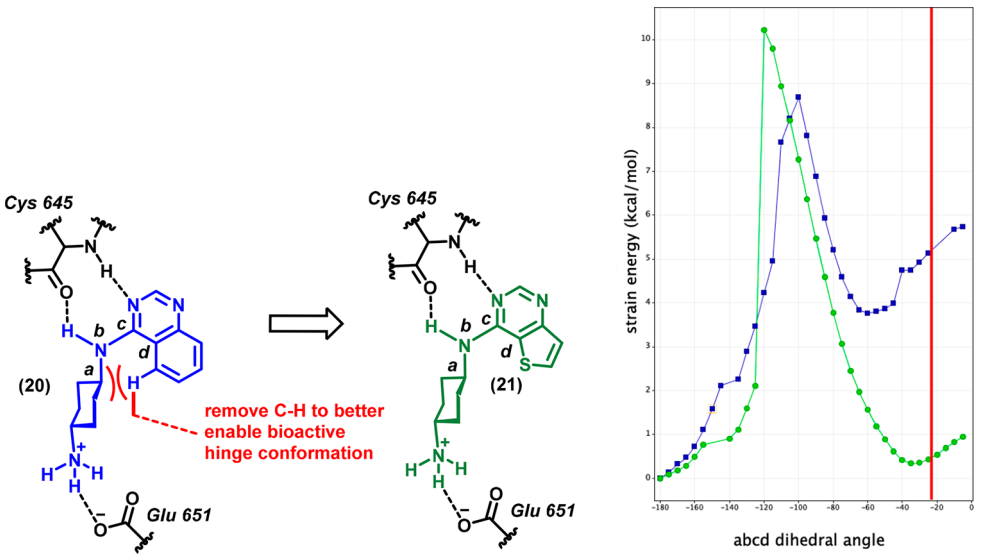

Figure 4. Quinazoline (blue, circle) to thienopyrimidine (green, square) design concept to improve bioactive hinge conformation and improve potency of polar headgroup incorporation. The quantum mechanical torsional profiles shown represent energies (kcal/mol) of the amino-quinazoline abcd dihedral angle when scanned from −180° to 0° in compounds **20** and **21.** Calculations were performed at the MP2/6-311+G**//HF/6-31G* level of theory with the PCM water solvent model using the Gaussian software package.[26] The crystal structure of **1** has an abcd torsion angle of ∼23° (labeled in red on plot above) to enable the formation of both a Glu651 salt bridge and a Cys645 hydrogen bond with the amino-quinazoline N−H.

Table 4. Thienopyrimidine Hinge SAR[a]

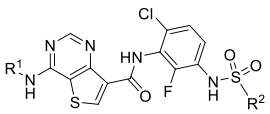

Compound	R^1	R^2	IRE1α-TR-FRET IC_{50} (μM)	IRE1α-RNase IC_{50} (μM)	XBP1-luc IC_{50} (μM)	BRaf Ki (μM)
22	H		0.0054	0.067	5.3	≤ 0.00008[b]
23		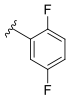	0.0051	0.024	0.32	0.0014
24			0.0039	0.03	0.39	0.055[b]
25			0.0044	0.022	0.12	0.11

[a]Data represent an average of ≥2 separate determinations. See the Supporting Information for standard deviations. [b]The potency was determined once.

observe that incorporating a *trans*-diaminocyclohexane substitution off the quinazoline A-ring amine of **2** was predicted to form a salt bridge contact with Glu651 and retained a similar fit and binding mode relative as the parent **2** (Figure 3a). A model of the same compound in BRaf suggests that the cyclohexyl ring of the newly added motif would clash with the BRaf Trp531 side chain and would not form a productive contact with the Braf His539 depending on its charge state and preferred rotamer (Figure 3b).

To explore this BRaf-sparing concept, a set of amino-quinazolines with basic amine polar head groups were prepared and evaluated (Table 3). Unfortunately, efforts in this area resulted in reduced IRE1α-TR-FRET binding potency and concomitant poor IRE1α cellular potency compared to the amino-quinazoline ligands in Tables 1 and 2. Nevertheless, we were encouraged by the *trans*-diaminocyclohexane containing compound **19**, which retained good IRE1α-TR-FRET binding potency and showed a substantial 4250-fold drop in BRaf binding potency and only a 19-fold decrease in XBP1-luc activity compared to **4**. This difference suggested BRaf-sparing was occurring, and it prompted us to further examine this concept toward maintaining reduced BRaf activity and improving IRE1α potency.

https://dx.doi.org/10.1021/acsmedchemlett.0c00344
ACS Med. Chem. Lett. XXXX, XXX, XXX−XXX

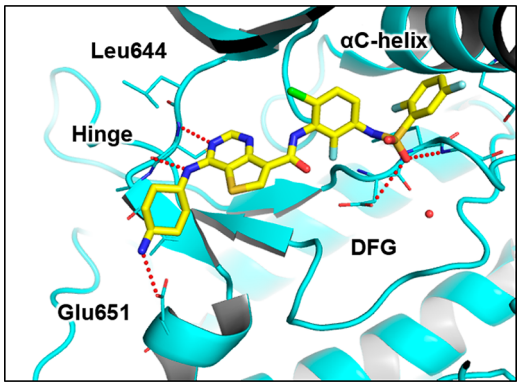

Figure 5. X-ray cocrystal structure of ligand **23** (yellow) in hIRE1α showing *trans*-diaminocyclohexane salt bridge formation with Glu651 (PBD = 6XDD, 2.40 Å).

The reduced IRE1α binding potency of **19** motivated us to consider conformational effects of the *trans*-diaminocyclohexane on predicted bioactive hinge conformation. The crystal structure of **1** with the similar *trans*-diaminocyclohexane moiety in the same location as **19** gives insight to the preferred dihedral angle of this moiety in the IRE1α protein. In this context, we considered replacing the quinazoline A/B ring system with the structurally related thienopyrimidine bicycling hinge which reduces the strain energy that would be expected in the bioactive conformation of the quinazoline due to the steric clash of the polar headgroup and the 5-position C−H of the quinazoline (Figure 4). Indeed, comparison of computed energies over a torsion scan of the simplified *trans*-diaminocyclohexane-quinazoline **20** and *trans*-diaminocyclohexane-thienopyrimidine **21** suggested that the predicted bioactive conformation of thienopyrimidine **21** has reduced strain energy compared to the predicted quinazoline **20** bioactive conformation. In addition, thienopyrimidines have been previously used as quinazoline surrogates in BRAF inhibitors and this together with the structure-based rationale outlined in Figure 4 motivated us to pursue this scaffold.[25]

As the torsion scan profiling provided a new promising hypothesis to improve IRE1α potency, a set of amino-substituted thienopyrimidines were synthesized (Table 4). As an initial validation of this hinge scaffold, the parent amino-thienopyrimidine **22** displayed similar IRE1α binding, XBP1 potency and BRaf activity as its amino-quinazoline counterpart **4** (Table 1).[27] Pleasingly, it was observed that the *trans*-diaminocyclohexane group was indeed better accommodated on the thienopyrimidine hinge compared to the quinazoline hinge supporting this conformation-based approach to optimize targeting of the Glu651 salt bridge (e.g., **23**). Importantly, we obtained a crystal structure of compound **23** in hIRE1α which showed the *trans*-diaminocyclohexane group engaging Glu651 in a salt bridge (Figure 5) which we presume contributes to the large gain in selectivity against BRaf, as the equivalent residue in BRaf is a histidine.

A brief survey of additional sulfonamide D-ring groups was performed to identify moieties that maintained XBP1 potency while also continuing to be BRaf sparing in the context of the *trans*-diaminocyclohexyl thienopyrimidine hinge system. In the end, these efforts led to the identification of **25** with good IRE1-XBP1 cellular potency and >1000-fold decrease in BRaf K_i potency vs **4** as a promising lead for further optimization. Compound **25** was also observed to be moderately stable in liver microsomes (CL_{HLM} = 9.5 mL/min/kg; CL_{MLM} = 34 mL/min/kg) and did not display significant hERG inhibition (1.1% inhibition at 1 μM; 6.4% inhibition at 10 μM). In addition, the related BRaf-sparing thienopyrimidine analogue **24** was also found to display good general kinase selectivity in a 220 member kinase panel (9/220 kinases inhibited >50% at 1 μM; see the Supporting Information for details).

In conclusion, we found that through appropriate substitution at the quinazoline 6-position a new pocket in IRE1α can be leveraged (through targeting of the P-loop His692 residue) to provide more than 100-fold improvement in cellular XBP1 potency. After extensive SAR studies at the quinazoline 6-position, it was determined that this new potency vector was ineffective toward reducing activity against the key BRaf kinase antitarget. Structural differences in the hinge regions of IRE1α and BRaf prompted design of amino-substituted quinazolines with the goal of targeting a salt bridge with Glu651 in IRE1α as a strategy to improve their BRaf selectivity profile. Torsional analyses then directed our attention toward deploying the related amino-thienopyrimidine hinge scaffold toward improved accommodation of the desired bioactive conformation. This strategy ultimately resulted in identification of *trans*-diaminocyclohexane substituted amino-thienopyrimidine **25** with good XBP1 potency and decreased BRaf binding potency as a promising lead for further optimization. Overall, this work exemplifies the importance of torsion profiles and ligand conformational considerations in design and showcases the potential of exploiting hinge connected polar head groups to achieve selectivity in kinase programs.

■ ASSOCIATED CONTENT

Supporting Information

The Supporting Information is available free of charge at https://pubs.acs.org/doi/10.1021/acsmedchemlett.0c00344.

Assay protocols, assay standard deviations, crystallographic information, characterization data for compounds **5**−**19** and **22**−**25**, synthetic procedures for compounds **14**, **19**, **22**, and **24**, QM torsion profiles for **20**−**21**, and kinase selectivity for **24** (PDF)

■ AUTHOR INFORMATION

Corresponding Authors

Ramsay E. Beveridge − *Paraza Pharma Inc., Montreal, QC, Canada H4S 2E1*; Email: ramsay.beveridge@parazapharma.com

Marie-Gabrielle Braun − *Genentech Inc., South San Francisco, California 94080-4990, United States*; orcid.org/0000-0002-5644-3711; Email: braun.mariegabrielle@gene.com

Authors

Heidi Ackerly Wallweber − *Genentech Inc., South San Francisco, California 94080-4990, United States*

Avi Ashkenazi − *Genentech Inc., South San Francisco, California 94080-4990, United States*

Maureen Beresini − *Genentech Inc., South San Francisco, California 94080-4990, United States*

Kevin R. Clark − *Genentech Inc., South San Francisco, California 94080-4990, United States*

Paul Gibbons − *Genentech Inc., South San Francisco, California 94080-4990, United States*

Elise Ghiro − *Paraza Pharma Inc., Montreal, QC, Canada H4S 2E1*

https://dx.doi.org/10.1021/acsmedchemlett.0c00344
ACS Med. Chem. Lett. XXXX, XXX, XXX−XXX

[§]**Susan Kaufman** − *Genentech Inc., South San Francisco, California 94080-4990, United States*
Alexandre Larivée − *Paraza Pharma Inc., Montreal, QC, Canada H4S 2E1*
Melissa Leblanc − *Paraza Pharma Inc., Montreal, QC, Canada H4S 2E1*
Jean-Philippe Leclerc − *Paraza Pharma Inc., Montreal, QC, Canada H4S 2E1*
Alexandre Lemire − *Paraza Pharma Inc., Montreal, QC, Canada H4S 2E1*
Cuong Ly − *Genentech Inc., South San Francisco, California 94080-4990, United States*
Joachim Rudolph − *Genentech Inc., South San Francisco, California 94080-4990, United States*
Jacob B. Schwarz − *Genentech Inc., South San Francisco, California 94080-4990, United States*
Sanjay Srivastava − *Paraza Pharma Inc., Montreal, QC, Canada H4S 2E1*
Weiru Wang − *Genentech Inc., South San Francisco, California 94080-4990, United States*
Liang Zhao − *Paraza Pharma Inc., Montreal, QC, Canada H4S 2E1*

Complete contact information is available at: https://pubs.acs.org/10.1021/acsmedchemlett.0c00344

Author Contributions

The manuscript was written through contributions of all authors. All authors have given approval to the final version of the manuscript.

Notes

The authors declare no competing financial interest.
[§]Susan Kaufman tragically passed away on July 29, 2020.

■ ACKNOWLEDGMENTS

We would like to thank the members of the synthetic chemistry and pharmacology teams at Wuxi Shanghai and Shanghai ChemPartner. We thank Genentech Analytical, Purification, DMPK, Pharmacology, Safety Assessment, and in vivo Studies Group colleagues for their contributions. In particular, we would like to acknowledge Chris Sneeringer for running BRAf assays. We thank staff at Advanced Light Source and Stanford Synchrotron Radiation Lightsource for assistance on data collection.

■ ABBREVIATIONS

IRE1α	inositol requiring enzyme 1-alpha
BRaf	serine/threonine-protein kinase BRaf
QM	quantum mechanics
UPR	unfolded protein response
XBP1	x-box binding protein-1
ER	endoplasmic reticulum
HLM	human liver microsomes
MLM	mouse liver microsomes.

■ REFERENCES

(1) Walter, P.; Ron, D. The Unfolded Protein Response: From Stress Pathway to Homeostatic Regulation. *Science* **2011**, *334*, 1081−1086.
(2) Rivas, A.; Vidal, R. L.; Hetz, C. Targeting the unfolded protein response for disease intervention. *Expert Opin. Ther. Targets* **2015**, *19*, 1203−1218.
(3) Hetz, C.; Chevet, E.; Oakes, S. A. Proteostasis control by the unfolded protein response. *Nat. Cell Biol.* **2015**, *17*, 829−838.
(4) Hetz, C.; Chevet, E.; Harding, H. P. Targeting the unfolded protein response in disease. *Nat. Rev. Drug Discovery* **2013**, *12*, 703−719.
(5) Xu, W.; Neckers, L. Gr(i)p the ER to stress out melanoma. *Cancer Cell* **2016**, *29*, 769−771.
(6) Raymundo, D. P.; Doultsinos, D.; Guillory, X.; Carlesso, A.; Eriksson, L. A.; Chevet, E. Pharmacological Targeting of IRE1 in Cancer. *Trends Cancer* **2020**, DOI: 10.1016/j.trecan.2020.07.006.
(7) Brancolini, C.; Iuliano, L. Proteotoxic Stress and Cell Death in Cancer Cells. *Cancers* **2020**, *12*, 2385−2412.
(8) Ojha, R.; Amaravadi, R. K. Targeting the unfolded protein response in cancer. *Pharmacol. Res.* **2017**, *120*, 258−266.
(9) Chen, Y.; Brandizzi, F. IRE1: ER stress sensor and cell fate executor. *Trends Cell Biol.* **2013**, *23*, 547−555.
(10) Mimura, N.; Fulciniti, M.l.; Gorgun, G.; Tai, Y. T.; Cirstea, D.; Santo, L.; Hu, Y.; Fabre, C.; Minami, J.; Ohguchi, H.; Kiziltepe, T.; Ikeda, H.; Kawano, Y.; French, M.; Blumenthal, M.; Tam, V.; Kertesz, N. L.; Malyankar, U. M.; Hokenson, M.; Pham, T.; Zeng, Q.; Patterson, J. B.; Richardson, P. G.; Munshi, N. C.; Anderson, K. C. Blockade of XBP1 splicing by inhibition of IRE1 is a promising therapeutic option in multiple myeloma. *Blood* **2012**, *119*, 5772−5781.
(11) Maly, D. J.; Papa, F. R. Druggable Sensors of the Unfolded Protein Response. *Nat. Chem. Biol.* **2014**, *10*, 892−901.
(12) Lu, M.; Lawrence, D. A.; Marsters, S.; Acosta-Alvear, D.; Kimmig, P.; Mendez, A. S.; Paton, A. W.; Paton, J. C.; Walter, P.; Ashkenazi, A. Opposing unfolded-protein-response signals converge on death receptor 5 to control apoptosis. *Science* **2014**, *345*, 98−101.
(13) Logue, S. E.; McGrath, E. P.; Cleary, P.; Greene, S.; Mnich, K.; Almanza, A.; Chevet, E.; Dwyer, R. M.; Oommen, A.; Legembre, P.; Godey, F.; Madden, E. C.; Leuzzi, B.; Obacz, J.; Zeng, Q.; Patterson, J. B.; Jager, R.; Gorman, A. M.; Samali, A. Inhibition of IRE1 RNase activity modulates the tumor cell secretome and enhances response to chemotherapy. *Nat. Commun.* **2018**, *9*, 1−14.
(14) Harnoss, J. M.; Le Thomas, A.; Shemorry, A.; Marsters, S. A.; Lawrence, D. A.; Lu, M.; Chen, Y.-C. A.; Qing, J.; Totpal, K.; Kan, D.; Segal, E.; Merchant, M.; Reichelt, M.; Ackerly Wallweber, H.; Wang, W.; Clark, K.; Kaufman, S.; Beresini, Maureen H.; Laing, Steven T.; Sandoval, W.; Lorenzo, M.; Wu, J.; Ly, J.; De Bruyn, T.; Heidersbach, A.; Haley, B.; Gogineni, A.; Weimer, R. M.; Lee, D.; Braun, M. G.; Rudolph, J.; Van Wyngarden, M. J.; Sherbenou, D. W.; Gomez-Bougie, P.; Amiot, M.; Acosta-Alvear, D.; Walter, P.; Ashkenazi, A. Disruption of IRE1α through its kinase domain attenuates multiple myeloma. *Proc. Natl. Acad. Sci. U. S. A.* **2019**, *116*, 16420−16429.
(15) Harnoss, J. M.; Le Thomas, A.; Reichelt, M.; Guttman, O.; Wu, T. D.; Marsters, S. A.; Shemorry, A.; Lawrence, D. A.; Kan, D.; Segal, E.; Merchant, M.; Totpal, K.; Crocker, L. M.; Mesh, K.; Dohse, M.; Solon, M.; Modrusan, Z.; Rudolph, J.; Koeppen, H.; Walter, P.; Ashkenazi, A. IRE1a Disruption in Triple-Negative Breast Cancer Cooperates with Antiangiogenic Therapy by Reversing ER Stress Adaptation and Remodeling the Tumor Microenvironment *Cancer*. *Cancer Res.* **2020**, *80*, 2368−2379.
(16) Papandreou, I.; Denko, N. C.; Olson, M.; Van Melckebeke, H.; Lust, S.; Tam, A.; Solo-Cordero, D. E.; Bouley, D. M.; Offner, F.; Niwa, M.; Koong, A. C. Identification of an IRE1alpha endonuclease specific inhibitor with cytotoxic activity against human multiple myeloma. *Blood* **2011**, *117*, 1311−1314.
(17) Ranatunga, S.; Tang, C.-H. A.; Kang, C. W.; Kriss, C. L.; Kloppenburg, B. J.; Hu, C.-C. A.; Del Valle, J. R. Synthesis of novel tricyclic chromenone-based inhibitors of IRE-1 RNase activity. *J. Med. Chem.* **2014**, *57*, 4289−4301.
(18) Sanches, M.; Duffy, N. M.; Talukdar, M.; Thevakumaran, N.; Chiovitti, D.; Canny, M. D.; Lee, K.; Kurinov, I.; Uehling, D.; Al-awar, R.; Poda, G.; Prakesh, M.; Wilson, B.; Tam, V.; Schweitzer, C.; Toro, A.; Lucas, J. L.; Vuga, D.; Lehmann, L.; Durocher, D.; Zeng, Q.; Patterson, J. B.; Sicheri, F. Structure and mechanism of action of the hydroxyl-aryl-aldehyde class of IRE1 endoribonuclease inhibitors. *Nat. Commun.* **2014**, *5*, 4202.
(19) Volkmann, K.; Lucas, J. L.; Vuga, D.; Wang, X.; Brumm, D.; Stiles, C.; Kriebel, D.; Der-Sarkissian, A.; Krishnan, K.; Schweitzer, C.;

Liu, Z.; Malyankar, U. M.; Chiovitti, D.; Canny, M.; Durocher, D.; Sicheri, F.; Patterson, J. B. Potent and selective inhibitors of the inositol-requiring enzyme 1 endoribonuclease. *J. Biol. Chem.* **2011**, *286*, 12743−12755.

(20) Waller, D. D.; Jansen, G.; Golizeh, M.; Martel-Lorion, C.; Dejgaard, K.; Shiao, T. C.; Mancuso, J.; Tsantrizos, Y. S.; Roy, R.; Sebag, M.; Sleno, L.; Thomas, D. Y. A covalent cysteine-targeting kinase inhibitor of IRE1 permits allosteric control of endoribonuclease activity. *ChemBioChem* **2016**, *17*, 843−851.

(21) Ghosh, R.; Wang, L.; Wang, E. S.; Perera, B. G. K.; Igbaria, A.; Morita, S.; Prado, K.; Thamsen, M.; Caswell, D.; Macias, H.; Weiberth, K. F.; Gliedt, M. J.; Alavi, M. V.; Hari, S. B.; Mitra, A. K.; Bhhatarai, B.; Schurer, S. C.; Snapp, E. L.; Gould, D. B.; German, M. S.; Backes, B. J.; Maly, D. J.; Oakes, A. A.; Papa, F. R. Allosteric inhibition of the IRE1α RNase preserves cell viability and function during endoplasmic reticulum stress. *Cell* **2014**, *158*, 534−548.

(22) Feldman, H. C.; Tong, M.; Wang, L.; Meza-Acevedo, R.; Gobillot, T. A.; Lebedev, I.; Gliedt, M. J.; Hari, S. B.; Mita, A. K.; Backes, B. J.; Papa, F. R.; Seeliger, M. A.; Maly, D. J. Structural and Functional Analysis of the Allosteric Inhibition of IRE1α with ATP-Competitive Ligands. *ACS Chem. Biol.* **2016**, *11*, 2195−2205.

(23) Wang, L.; Perera, B. G.; Hari, S. B.; Bhhatarai, B.; Backes, B. J.; Seeliger, M. A.; Schurer, S. C.; Oakes, S. A.; Papa, F. R.; Maly, D. J. Divergent allosteric control of the IRE1alpha endoribonuclease using kinase inhibitors. *Nat. Chem. Biol.* **2012**, *8*, 982−989.

(24) Harrington, P. E.; Biswas, K.; Malwitz, D.; Tasker, A. S.; Mohr, C.; Andrews, K. L.; Dellamaggiore, K.; Kendall, R.; Beckmann, H.; Jaeckel, P.; Materna-Reichelt, S.; Allen, J. R.; Lipford, J. R. Unfolded Protein Response in Cancer: IRE1α Inhibition by Selective Kinase Ligands Does Not Impair Tumor Cell Viability. *ACS Med. Chem. Lett.* **2015**, *6*, 68−72.

(25) Mathieu, S.; Gradl, S. N.; Ren, L.; Wen, Z.; Aliagas, I.; Gunzner-Toste, J.; Lee, W.; Pulk, R.; Zhao, G.; Alicke, B.; Boggs, J. W.; Buckmelter, A. J.; Choo, E. F.; Dinkel, V.; Gloor, S. L.; Gould, S. E.; Hansen, J. D.; Hastings, G.; Hatzivassiliou, G.; Laird, E. R.; Moreno, D.; Ran, Y.; Voegtli, W. C.; Wenglowsky, S.; Grina, J.; Rudolph, J. Potent and selective aminopyrimidine-based B-Raf inhibitors with favorable physicochemical and pharmacokinetic properties. *J. Med. Chem.* **2012**, *55*, 2869−2881.

(26) Frisch, M. J.; Trucks, G. W.; Schlegel, H. B.; Scuseria, G. E.; Robb, M. A.; Cheeseman, J. R.; Scalmani, G.; Barone, V.; Petersson, G. A.; Nakatsuji, H.; Li, X.; Caricato, M.; Marenich, A.; Bloino, J.; Janesko, B. G.; Gomperts, R.; Mennucci, B.; Hratchian, H. P.; Ortiz, J. V.; Izmaylov, A. F.; Sonnenberg, J. L.; Williams-Young, D.; Ding, F.; Lipparini, F.; Egidi, F.; Goings, J.; Peng, B.; Petrone, A.; Henderson, T.; Ranasinghe, D.; Zakrzewski, V. G.; Gao, J.; Rega, N.; Zheng, G.; Liang, W.; Hada, M.; Ehara, M.; Toyota, K.; Fukuda, R.; Hasegawa, J.; Ishida, M.; Nakajima, T.; Honda, Y.; Kitao, O.; Nakai, H.; Vreven, T.; Throssell, K.; Montgomery, J. A., Jr.; Peralta, J. E.; Ogliaro, F.; Bearpark, M.; Heyd, J. J.; Brothers, E.; Kudin, K. N.; Staroverov, V. N.; Keith, T.; Kobayashi, R.; Normand, J.; Raghavachari, K.; Rendell, A.; Burant, J. C.; Iyengar, S. S.; Tomasi, J.; Cossi, M.; Millam, J. M.; Klene, M.; Adamo, C.; Cammi, R.; Ochterski, J. W.; Martin, R. L.; Morokuma, K.; Farkas, O.; Foresman, J. B.; Fox, D. J. *Gaussian 09*, rev. E.01; Gaussian, Inc., Wallingford, CT, 2013.

(27) The potency of the most potent thienopyrimidines tested in the kinase focused library (compound **27**) is included in the Supporting Information:

R_1=H and R_2=

https://dx.doi.org/10.1021/acsmedchemlett.0c00344
ACS Med. Chem. Lett. XXXX, XXX, XXX−XXX